1 **Criticality as a determinant of integrated information Φ in human brain**

2 **networks**

3

4 Hyoungkyu Kim[1,2], Anthony G. Hudetz[1,2,3,], George A. Mashour[1,2,3], UnCheol Lee[1,2*]

5 *[1]Department of Anesthesiology, University of Michigan Medical School, Ann Arbor, MI,*

6 *USA*

7 *[2]Center for Consciousness Science, University of Michigan Medical School, Domino's*

8 *Farms, P.O. Box 385, Ann Arbor, MI, USA*

9 *[3] Neuroscience Graduate Program, University of Michigan, Ann Arbor, MI, USA*

10
11
12
13 *** Correspondence:**
14 UnCheol Lee
15 uclee@med.umich.edu
16
17
18

20

21 Abstract

22 Integrated information theory (IIT) postulates that consciousness arises from the cause-effect

23 structure of a system but the optimal network conditions for this structure have not been

24 elucidated. In the study, we test the hypothesis that network criticality, a dynamically balanced

25 state between a large variation of functional network configurations and a large constraint of

26 structural network configurations, is a necessary condition for the emergence of a cause-effect

27 structure that results in a large Φ, a surrogate of integrated information. We also hypothesized

28 that if the brain deviates from criticality, the cause-effect structure is obscured and Φ diminishes.

29 We tested these hypotheses with a large-scale brain network model and high-density

30 electroencephalography (EEG) acquired during various levels of human consciousness during

31 general anesthesia. In the modeling study, maximal criticality coincided with maximal Φ. The

32 constraint of the structural network on the functional network is maximized in the maximal

33 criticality. The EEG study demonstrated an explicit relationship between Φ, criticality, and level

34   of consciousness. Functional brain network significantly correlated with structural brain network

35   only in conscious states. The results support the hypothesis that network criticality maximizes

36   Φ.

37

38   **Introduction**

39   Integrated information theory (IIT) proposes that consciousness equates with integrated

40   information in a system and the integrated information is maximized when integration and

41   differentiation of the systems' components are balanced. IIT proposes algorithmic methods to

42   identify the differentiated parts of a system and quantify the integrated information across the

43   parts [1–6]. Φ is a measure of complexity of the cause-effect structure of the minimum

44   information partition among all possible partitions. However, in a dynamic system such as the

45   brain, the optimal conditions under which the cause-effect structure—that is, the basis of

46   integrated information— arises has not been elucidated. In this study, we hypothesized that

47   network criticality, a balanced state between a large variation of functional network

48   configurations and a large constraint of structural network configurations, may be the basis of

49   the high Φ in conscious brains.

50   Criticality was originally introduced for studying phase transition in physics, which was simply

51   defined as a balanced state between order and disorder in the activities of the elements that

52   make up a system [7,8]. This property has been observed broadly in physical and non-physical

53   systems and has been suggested as an optimal state for information storage, transmission, and

54   integration with high susceptibility to external stimuli [9–13]. In particular, several computational

55   modeling and empirical studies suggest that the brain dynamics associated with consciousness

56   reside near a critical state [14–19]. Furthermore, recent studies have attempted not only to

57   identify whether the conscious brain resides near the critical state but also to understand

58   systematically how various types of brain perturbations (sleep, anesthesia, and traumatic

59   injuries) lead to a deviation from criticality [9,20–23]. Such approaches introduce the criticality

60   hypothesis as a theoretical framework to study pharmacological and pathological states of

61   unconsciousness, such as anesthesia and coma. Regarding the characteristics of a critical state

62   such as highly informative, highly susceptible, highly efficient, and highly integrative, criticality

63   shares many commonalities with the brain state that IIT proposes as conducive to

64   consciousness. However, the relationship between criticality, Φ, and human consciousness has

65   not been demonstrated explicitly.

66 To identify a relationship between criticality and Φ, we analyzed computationally a large-scale

67 human brain network model adjusting criticality with a control parameter. The criticality was

68 defined using the pair correlation function (PCF), a surrogate measure of susceptibility [24]. The

69 relative change of Φ across states was estimated with $\bar{\Phi}$, a surrogate measure of Φ that we

70 developed for high-density EEG. Empirically, we modulated the level of human consciousness

71 in a stepwise manner with an anesthetic and calculated both $\bar{\Phi}$ and PCF from continuous EEG

72 data. From the modeling study and EEG analysis, we were able to quantitatively study the

73 relationship between Φ, criticality, and consciousness, and suggested network criticality as a

74 necessary condition for a high Φ in human brain networks.
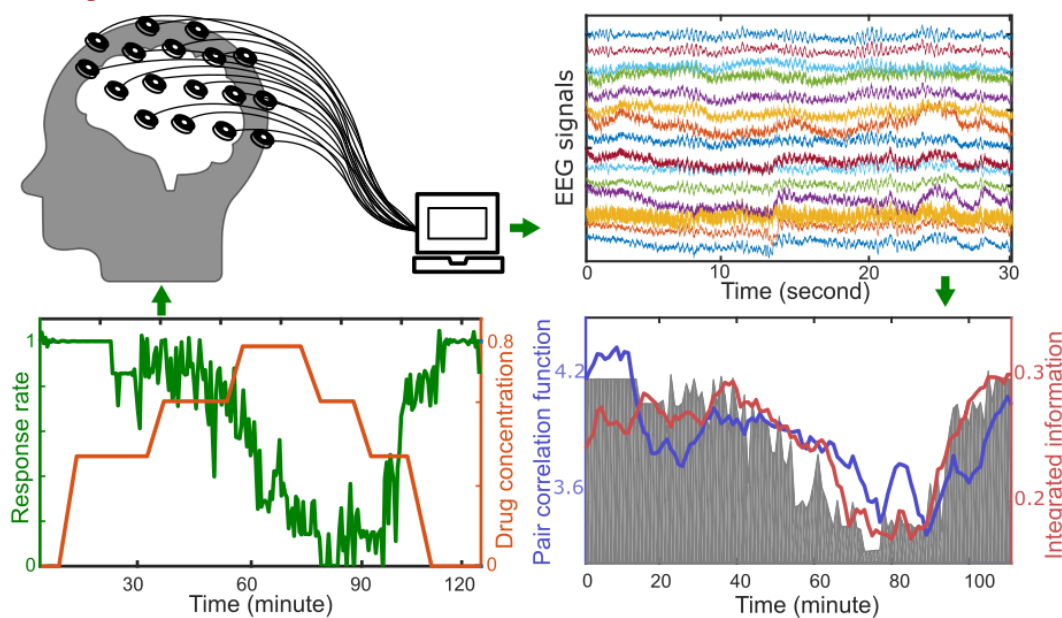
A. Ocsillator model in brain network

Equation of Kuramoto model

$$\dot{\theta}_j(t) = \omega_j + S\sum_{k=1}^{N} A_{jk}\, sin\{\theta_k(t-\tau_{jk}) - \theta_j(t)\}, \quad j = 1, 2, \dots, N$$
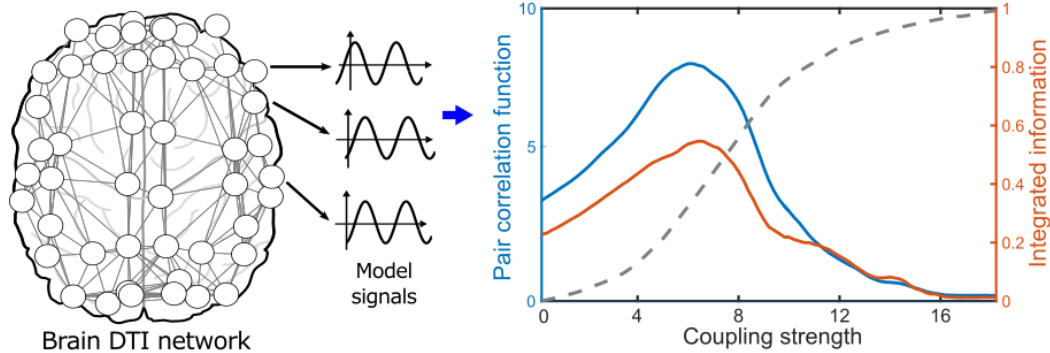
B. Analysis in human EEG

EEG signals from sevoflurane-induced unconsciousness

Figure 1. Schematic flow diagram for studying the relationship between criticality (defined as pair correlation function, PCF), integrated information (Φ) and human consciousness. (A) Model study: a simple coupled oscillator model (Kuramoto model) was implemented on an anatomically informed human brain network structure constructed from diffusion tensor imaging (DTI). The Φ was calculated while modulating the level of criticality with a control parameter (coupling strength). The level of criticality was defined using PCF, a susceptibility measure, of the simulated brain activity. (B) Empirical study: 64-channel EEG data derived from seven healthy volunteers were recorded while gradually increasing sevoflurane concentration from 0.4% to 0.6% to 0.8%, then decreasing it from 0.8% to 0.6% to 0.4%. The changes of PCF and Φ were compared with the response rate to verbal commands.

85   **Methods**

86   **Ethics Statement:** This study was conducted at the University of Michigan Medical School and

87   approved by the Institutional Review Board (HUM00061087); after careful discussion, written

88   informed consent was obtained from all participants.

89   **Human brain network model:** Many recent studies have successfully applied Kuramoto/Stuart-

90   Landau models to the brain in order to understand the organizational principles of multiscale

91   brain function, surrogates of information flow, and complex dynamics at the whole brain network

92   level [25–27]. Similarly, we hypothesized that the application of simple oscillatory models, which

93   can modulate the criticality with a control parameter, to an anatomically informed brain network

94   structure could inform the relationship between brain network criticality and integrated

95   information.

96   We used a large-scale brain network model that implements a coupled simple oscillator model

97   on the scaffold of an anatomically informed human brain network structure. The human brain

98   network consists of 78 parcels of the cerebral cortex constructed from diffusion tensor imaging

99   (DTI) of 80 young adults [28].

100
$$\dot{\theta}_j(t) = \omega_j + S \sum_{k=1}^{N} A_{jk} sin\left(\theta_k(t - \tau_{jk}) - \theta_j(t)\right) \quad, j = 1, 2, \ldots, N. \qquad (1)$$

101   Here S is the coupling strength between oscillators and A_{jk} denotes the anatomical connections

102   between oscillator j and k, yielding 1 if a connection exists and 0 otherwise. τ_{jk} is the time delay

103   between node j and k. $\theta_j(t)$ is the phase of oscillator j at time t. ω_j is the intrinsic frequency of

104   oscillator j.

105   **Simulation procedures:** All parameters for the models were set to simulate alpha oscillations

106   in the brain. Alpha oscillation models have successfully explained empirically observed brain

107   network behaviors such as functional connectivity, traveling waves, and network state

108   transitions based on electroencephalography (EEG) and magnetoencephalography (MEG)

109   [25,26,29–37]. Thus, alpha oscillations were analyzed to understand the behaviors of Φ and the

110   criticality at the brain network level. The natural frequencies of the oscillators in our simulation

111   were given as a Gaussian distribution around 10 Hz with a standard deviation of 0.5 Hz. Time

112   delay was set proportional to the physical distances between nodes with a propagation speed of

113   8.6m/s [38]. The coupling strength between the oscillators was continuously changed from 0 to

114   18. In each parameter set, 100 configurations were simulated and the results were averaged

115   over all configurations.

116   **Experimental procedures:** We conducted a secondary analysis of high-density EEG data from

117   a study of sevoflurane-induced unconsciousness in humans; the details of the experiment can

118   be found in the supplementary text of this article and the previously published Blain-Moraes et al

119   [39]. The current study tested different hypotheses and, unlike the original study, included

120   computational analyses of brain network models.

121   **Sevoflurane dataset:** 64-channel EEG were recorded from seven healthy volunteers as

122   sevoflurane concentrations in high-flow oxygen (8 L/min) were gradually increased from 0.4% to

123   0.6% to 0.8% (the average range at which unconsciousness was induced) or beyond, then

124   decreased from 0.8% to 0.6% to 0.4%. The EEG was recorded with eyes closed. The loss and

125   recovery of consciousness were defined as the loss and recovery of response to the verbal

126   command 'squeeze your left [or right] hand twice,' on a recorded loop every 30 seconds, with

127   right/left hand commands randomized.

128   Average reference was used for re-referencing and the windowed sinc-FIR filter (in the MATLAB

129   toolbox from EEGLAB) was used to avoid a possible shifting of the signal. We analyzed 12-

130   second-long EEG epochs with 1-minute-long moving windows.

131   **Criticality:** Criticality, a boundary state between order and disorder, has long been proposed to

132   play an important role in neural dynamics and brain function. Empirical evidence supports the

133   hypothesis that the brain operates at or near the critical point, not only at the neuronal network

134   level [22,40,41], but also at the large-scale or global network level [9,12,42–44]. Until now, most

135   studies have focused on scale-free behavior, showing power law distribution of empirically

136   observed variables. It has also been recently proposed that high correlation between functional

137   and structural brain networks [14,23,25,26,45] and a large pair correlation function (PCF)

138   [24,46] is evidence of criticality. In both the brain network model and empirical EEG data, we

139   estimated criticality with PCF, which is the variance of global phase synchronization and is

140   equivalent to susceptibility in statistical physics

141     $$PCF = N\left\{< Re^2[z(t)] >_t - < Re[z(t)] >_t^2\right\} \qquad (2)$$

142   where Re[*z(t)*] is the real part of the *z(t)* in Eq. (3).

143     $$z = r\,e^{i\Psi} = \frac{1}{N}\sum_{j=1}^{N} e^{i\theta_j} \qquad (3)$$

144 where Ψ is the order parameter phase. The absolute value $r = |z|$ represents the degree of

145 synchronization. The r is equal to zero when the phases of nodes are uniformly distributed and

146 one when all the nodes have the same phase.

147 **Calculation of $\bar{\Phi}$:** IIT defines integrated information (Φ) as the effective information (φ) of the

148 minimum information partition (MIP) in a system [1–3,5,47]. The MIP is also defined as the

149 partition having minimum effective information among all possible partitions.

150 $$\Phi [X;x] = : \varphi [X;x, MIP(x)] \qquad (4)$$

151 $$MIP (x) = : \arg \min\{ \varphi (X;x , P) \} \qquad (5)$$

152 where X is the system, x is a state, and P is a partition P=$\{M^1, ..., M^r\}$.

153 Identifying the MIP requires searching all possible partitions and comparing their effective

154 information φ. This is the most time-consuming and computationally demanding process in the

155 application to high-density EEG. Furthermore, considering the fact that EEG data recorded

156 during anesthetic state transitions are non-Gaussian and continuous time series, we used the

157 $\widetilde{\Phi}_{AR}$ as a measure of integrated information [48]. The computed $\widetilde{\Phi}_{AR}$ values from original signals

158 were compared with the $\widetilde{\Phi}_{AR}$ values of surrogate data sets, and non-significant $\widetilde{\Phi}_{AR}$ values were

159 set as zero.

160 Although many improvements have been made in the algorithms of Φ over the last decade, the

161 computation time is still unrealistic because of the need to search an enormous number of

162 partitions to identify the MIP. In our previous study, we proposed a surrogate measure $\bar{\Phi}$ to

163 circumvent the explosive computational time of Φ for high-density EEGs. $\bar{\Phi}$ estimates the

164 relative change of Φ across states by considering the average feature of many small sample

165 units rather than trying to identify the MIP and its effective information for all EEG channels. A

166 sample unit consists of a small number of EEG channels randomly selected from 64 channels

167 and the total number of sample units is taken as large enough to represent the behavior of the

168 entire high-density EEG montage. In this study, we limited our interest only to the relative

169 changes of Φ values across states, rather than attempting to calculate the exact Φ value for

170 each brain state, which would be impossible to measure using the superficial and spatially

171 imprecise brain activity recorded by EEGs.

172 For each sample unit, we were able to calculate the MIP and its effective information—that is,

173 the Φ of the sample unit. For instance, in this study, we selected 8 random EEG channels for a

174 sample unit and acquired 200 sample units that were randomly selected from the baseline

175   states. The same 200 sample units determined in the baseline were then compared across EEG

176   windows to investigate the increase or decrease of Φ values. Since the number of possible

177   bipartitions of 8 channels is $\sum_{k=1}^{4} C(8,k) = 162$, where C stands for the combination of k unique

178   elements chosen from eight possible elements, calculating Φ for all EEG windows of seven

179   subjects during state transitions is possible within a relatively short computational time.

180   The average $\bar{\Phi}$ is defined as follows.

181 $$\bar{\Phi} = \frac{1}{k}\sum_{i=1}^{k} \Phi_i(n) - \frac{1}{k}\sum_{i=1}^{k} median(\Phi_{surr(i)}(n)) \qquad (6)$$

182   where n is the number of EEG channels for a sample unit and k is the number of sample units of

183   the n EEG channels. $\Phi_i(n)$ measures the effective information of MIP for the n EEG channels,

184   by definition, the integrated information of the sample unit. Here, we chose n=8 and k=200

185   following our previous study [49]. $\Phi_{surr}(n)$ is the spurious $\Phi_i(n)$ estimated from randomly

186   shuffled EEG data sets. Subtracting the randomness, $\bar{\Phi}$ reflects the average integrated

187   information of 200 sample units taken from the high-density EEG data that exceeds the spurious

188   information integrated from the surrogate data. Since $\bar{\Phi}$ estimates the relative change of Φ, it is

189   appropriate for our purposes to detect the maximum Φ to compare with the maximum criticality.

190   **Functional connectivity:** Phase Lag Index (*PLI*), a measure of phase locking between two

191   signals, was used to define the functional connectivity in the EEG network [50]. We chose a

192   Hilbert transform to extract the instantaneous phase of the EEG from each channel and

193   calculate the phase difference $\Delta\theta_{ij}(t)$ between channels i and j, where $\Delta\theta_{ij}(t) = \theta_i(t) - \theta_j(t)$, t

194   = $1,2,…,n$, and n is the number of samples within one epoch. PLI_{ij} between two nodes i and j is

195   then calculated using equation (7):

196 $$PLI_{ij} = |< sign(\Delta\theta_{ij}(t)) >|, \quad 0 \leq PLI_{ij} \leq 1. \qquad (7)$$

197   Here, the sign() function yields: 1 if $\Delta\theta_{ij}(t) > 0$; 0 if $\Delta\theta_{ij}(t) = 0$; and -1 if $\Delta\theta_{ij}(t) < 0$. The mean

198   < > is taken over all $t=1,2,…,n$. If the instantaneous phase of one signal is consistently ahead of

199   the other signal, the phases are considered locked and $PLI_{ij} \approx 1$. However, if the signals

200   randomly alternate between a phase lead and phase lag relationship, there is no phase locking

201   and $PLI_{ij} \approx 0$.

202   **Surrogate data:** To control for spurious connectivity of EEG, 20 surrogate data sets were

203   generated with a random shuffling method, in which a time point is randomly chosen in each

204   EEG channel; the EEG epochs are then shuffled before and after the time point. The shuffled

205   data have the same amplitude distribution and power spectrum of the original EEG, but there

206   are disruptions of the original connectivity between two EEG signals.

207   **Network construction:** We expected that different EEG frequency bands and different states

208   would have different levels of spurious connectivity [51]. Thus, after subtracting the median *PLI*

209   of 20 surrogate data sets, if the remaining *PLI* was larger than 0.1 then the connectivity of two

210   EEG signals was set as 1; otherwise, it was set as 0. The threshold (0.1) was chosen to avoid

211   isolated nodes in the EEG network in the baseline states. The node degree of an EEG channel

212   was defined as the number of functional links in the network.

213   **EEG simulation:** To test if the *PLI* network of EEG in conscious states is similar to the

214   structural brain network in a critical state, we simulated 78 source signals in the structural brain

215   network in a critical state and projected it into the 64 sensor signals on the scalp. We could then

216   directly compare the *PLI* networks of EEG and the *PLI* network of the simulated EEG (; the 64

217   sensor signals on the scalp). The signals generated from the Kuramoto model and structural

218   brain network represent source activities of the brain, which are under the surface of where

219   EEG is measured. In reality, the electrical potentials generated by the neural activity in the brain

220   conduct outwards through brain tissue and the skull and finally appear at the scalp surface

221   where the EEG signal is measured. In order to compare experimental EEG and the model

222   signals, we generated surface level signals from the simulated source signals. We used three

223   concentric spherical head models; the three layers consist of the brain, skull, and scalp. The

224   conductivity of the three layers was set to be 0.33, 0.0042, and 0.33 S/m, respectively [52]. The

225   source activity was represented as a dipole moment. The coordinate of the dipole moment in

226   the brain was determined by the region's standard coordinates and the orientation of the dipole

227   moment was randomly assigned. The forward model simulation was conducted by using the

228   Field Trip Toolboox [53].

229   **Statistical Analysis:** We performed one-way ANOVA ("anova1.m", MATLAB toolbox) with

230   Tukey-Kramer correction ("multcompare.m" with alpha = 0.05 and ctype = "tukey-kramer" in

231   MATLAB) for the comparison of the PCF and $\bar{\Phi}$ among different states. The statistical tests

232   were carried out for the modeling and empirical analysis separately. The adjusted P-values of

233   0.05 or lower (*P < 0.05, **P < 0.01, and ***P < 0.001) were considered to be statistically

234   significant (S1 Table and S2 Table).

235

236 **Results**

237

238 **Model Study: Correlation between Criticality and $\bar{\Phi}$**

239 We simulated various brain network dynamics by adjusting the control parameter (i.e., coupling

240 strength). First, we determined the critical state of the model by identifying the coupling strength

241 that yielded a maximum criticality. The criticality of the system was defined by PCF, which

242 reflects the susceptibility of the brain network dynamics to perturbation. As the coupling strength

243 of the network was increased, the PCF reached a maximum at an intermediate coupling

244 strength, while the order parameter increased monotonically (dotted line in Figure 2A). In Figure

245 2A, we illustrate the intermediate coupling strength (blue region) as the critical state of this brain

246 network model and selected an incoherent (green region) and highly synchronized (red region)

247 states of lower PCFs as a supercritical and subcritical state, respectively. The $\bar{\Phi}$ value was also

248 maximized at a point between sub- and supercritical states, at a similar coupling strength that

249 corresponds to the maximum PCF.

250 Here, we assumed that the maximum $\bar{\Phi}$ may arise due to the balance between the large

251 variation of functional network configurations and the large constraints of structural network

252 configurations, as a characteristic of a critical state. The disrupted balance in an incoherent or

253 highly synchronized brain network results in a small $\bar{\Phi}$. Figure 2B presents the functional brain

254 networks based on the phase lag index (*PLI*). The functional connectivity at the maximum PCF

255 (in the critical state) resembles the structural brain network of DTI, whereas the functional

256 connectivity at the lower PCFs (in the sub-and supercritical states) are relatively homogeneous

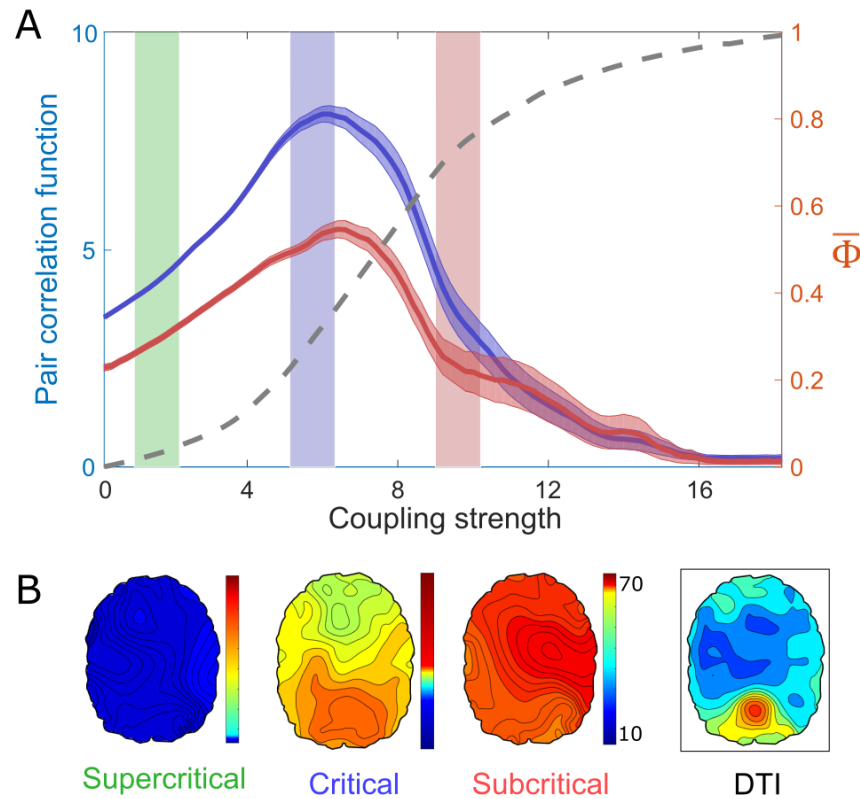257 and not similar with the structural brain network.

258

Figure 2. Criticality, $\bar{\Phi}$, and structured functional connectivity in the brain network. (A) When modulating the coupling strength (a control parameter), the maximum $\bar{\Phi}$ coincides with the maximum criticality, as measured by the pair correlation function (PCF), while the order parameter (dotted line) increases in a monotonic way. (B) Only in the critical state (blue region in Figure 2A), a salient structured functional connectivity, which resembles the structural brain network, emerges in the brain network. Color bar indicates the node degree.

A Network Mechanism of the Maximal $\bar{\Phi}$ in a Critical State

In a critical state, a network synchronization is balanced by incoherent and synchronous connections through partial phase locking. At a coarse-grained level, the distribution of incoherent and synchronous connections is shaped by the network topology; oscillations at the nodes with dense connections become slower and more synchronous, while oscillations at the nodes with sparse connections are faster and incoherent [25,26]. As a consequence, a coarse-grained functional network resembles a structural network in a critical state [14,54,55].

275   Figure 3A presents the Spearman correlation coefficients between the node degrees (in the

276   structural brain network) and the *PLI*s of the 78 nodes (in the functional brain network) as

277   coupling strength increases. The Spearman correlation coefficient is at a maximum in the critical

278   state (blue region), while both the super- and subcritical states (green and red regions,

279   respectively) are associated with smaller correlations. The results imply that the constraint of the

280   structural network on a functional network is maximized in the critical state, with higher degree

281   nodes having a larger *PLI*. Figure 3B presents the scatter plots of the *PLIs* versus the node

282   degrees of the 78 nodes in the three states. A large positive correlation coefficient appears only

283   in the critical state (Figure 3B blue, r=0.57, p-value < 0.001). However, the large correlation

284   does not mean that the functional network is static. Figure 3C presents the temporal evolution of

285   the Spearman correlation coefficients between the instantaneous phases of alpha oscillations in

286   the functional brain network and the node degrees in the structural brain network for the three

287   states. The varying correlation coefficients indicate the temporal change of the phase lead-lag

288   relationships among 78 brain regions upon the structural brain network. The large variation of

289   functional networks is one of the characteristics of a critical state and measured by a large PCF.

290   As a result, the large variation of the functional brain network at a small-time scale (~ seconds)

291   (Figure 3C) under the large constraint from the structural brain network (Figure 3B) in a large

292   time scale (~ minutes) in the critical state may be the network condition for the maximal $\overline{\overline{\Phi}}$ in the
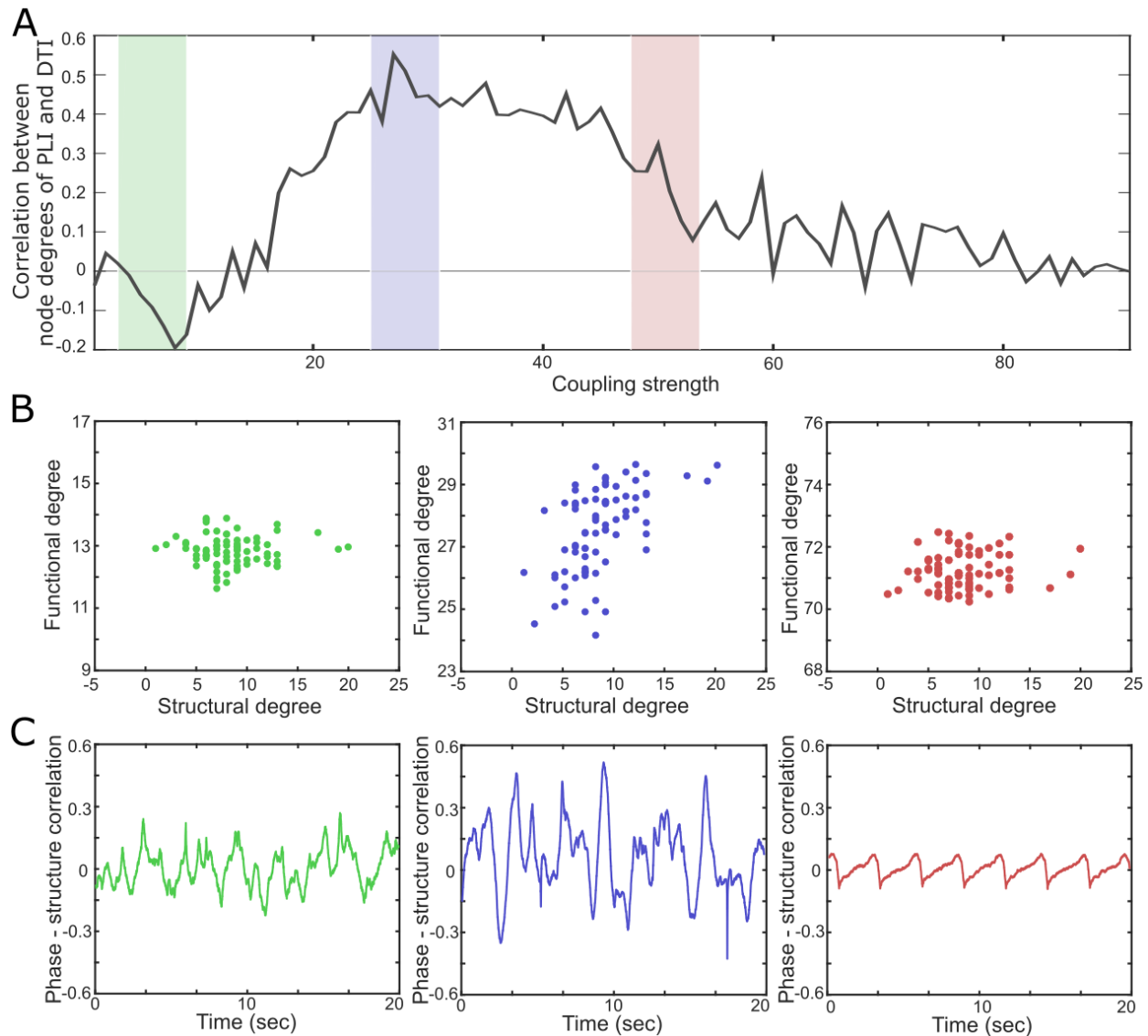
293   brain network.

294

Figure 3. Correlations between the functional and structural brain networks near to and far from a critical state. (A) The Spearman correlation coefficient between the 78 phase lag index (*PLI*) values in the functional brain network and the 78 node degrees in the structural brain network is maximal in the critical state (black line, blue shaded region). (B) The scatter plots (the 78 *PLI* values versus the 78 node degrees) for the supercritical (green), critical (blue), and subcritical (red) states. The large correlation in the critical state implies a large constraint of the structural network on the functional network. (C) The Spearman correlation coefficients between the instantaneous phases of alpha oscillations and the node degrees of the 78 nodes in the structural brain network. The large temporal variation indicates a large repertoire of functional connectivity, which is a characteristic of a critical state.

306 **EEG study: Correlation between Criticality, $\bar{\Phi}$, and Human Consciousness**

307 To investigate the relationship between criticality, integrated information, and level of human

308 consciousness, we compared the PCF and $\bar{\Phi}$ of high-density EEG and the response rate during

309 general anesthesia. The behavioral response rate, which is inversely proportional to the drug

310 concentration, was used as a surrogate for the level of consciousness. In figure 4A, the

311 conscious resting state and the conscious recovery state have a higher PCF and $\bar{\Phi}$ than in the

312 unconscious states. For the continuous EEG data, the change of PCF correlates with the

313 change of $\bar{\Phi}$. Moreover, both the measures reflect the response rate during the significant state

314 transition. These results are consistent with the model prediction and empirically demonstrate

315 for the first time a direct relationship between PCF, $\bar{\Phi}$, and the level of human consciousness.

316 The model study also predicted a large correlation of the structural brain network with the

317 functional brain network in consciousness, which corresponds to the functional brain network in

318 a critical state. However, since we recorded only the scalp EEG, we were not able to test the

319 correlation between functional (*PLI*) and structural (node degree) brain networks. Instead, we

320 compared the *PLI* networks of the EEG and a simulated EEG. For the simulation of EEG in the

321 conscious state, we first simulated the source signals in the structural brain network in a critical

322 state (the same simulation in Figure 2 and 3) and then projected the source signals onto the

323 scalp (see the Method in details). If the model prediction is correct, both the *PLI* networks

324 should be largely correlated.

325 Indeed, we found high Spearman correlation coefficients between the *PLI* network of the EEG in

326 the conscious states and the *PLI* network of the simulated EEG in a critical state. This

327 correlation decreases along with the reduced response rate in the unconscious states (Figure

328 4B). The high correlation coefficients in conscious states indicate a strong constraint of the

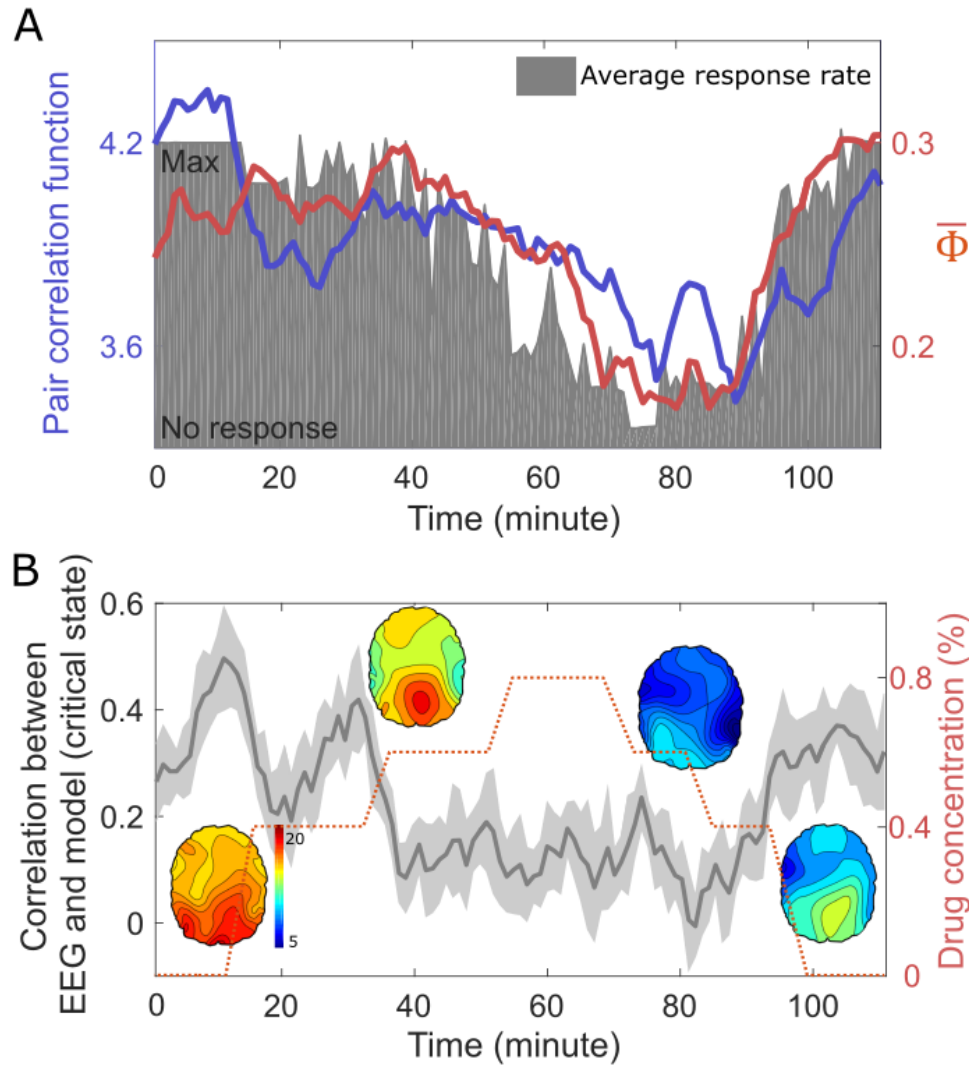329 structural brain network on the EEG.

330

331

332   Figure 4. Criticality, integrated information, and level of human consciousness during general

333   anesthesia. (A) The PCF and $\bar{\Phi}$ of 64-channel EEG correlate with the response rate (grey area),

334   which was modulated with increasing anesthetic concentrations. (B) The Spearman correlation

335   coefficients between the *PLI* networks of the EEG and the simulated EEG based on the

336   anatomical brain network and critical state. The conscious states (baseline, induction, and

337   recovery) show larger correlations, which implies a stronger constraint of the structural brain

338   network on the EEG in conscious states. As a result, the balance between the large constraint

339   of the structural brain network and the large repertoire (i.e., large PCF) of the functional brain

340   network may be the network basis of the large $\bar{\Phi}$ of EEG in the conscious brains.

341

342

343 **Discussion**

344 **Summary of the findings:** In this paper, we performed a computational modeling and EEG

345 data analysis to study the relationship between integrated information, criticality, and level of

346 human consciousness. In the modeling study, we simulated the brain network activities near

347 and far from a critical state and quantified the criticality and integrated information with PCF and

348 $\bar{\Phi}$. We found that when the brain network reaches a maximal PCF, the $\bar{\Phi}$ is also maximized

349 under the largest constraint of the structural brain network (that is, with the largest correlation

350 between the functional and structural brain networks). To verify the modeling results, we

351 gradually modulated the level of consciousness in humans with a general anesthetic and

352 compared the PCF and $\bar{\Phi}$ of high-density EEG with the behavioral response rate. We found

353 that, in the conscious resting states, the subjects have the highest PCF and $\bar{\Phi}s$ when the

354 behavioral response rates are highest. We also showed that the functional brain network of

355 EEGs in conscious states largely correlates with the functional brain network of the simulated

356 EEGs, which were modeled to reflect the underlying structural brain network in a critical state.

357 From both the modeling study and EEG analysis, we propose that the balance between the

358 large variation of functional brain network (as measured as the large PCF) and the large

359 constraint from the structural brain network in a critical state is a necessary condition to

360 generate the high $\bar{\Phi}$ of conscious states.

361 **Criticality and maximal $\bar{\Phi}$:** IIT's composition principle states that any subset of elements

362 within a system can be a mechanism of the system if the intrinsic cause-effect power is

363 irreducible [1,3]. Furthermore, the set of all mechanisms and their constraints within the system

364 comprises a system's cause-effect structure. Algorithmically, the intrinsic cause-effect structure

365 can be identified by the effective information among partitions (φ), with the integrated

366 information of a system (Φ) defined by the information transmission of the minimal information

367 bipartitions. However, in the application to our brain network model, since we did not give any

368 cause-effect structure initially, a non-zero $\bar{\Phi}$ may emerge through only the interaction of 78

369 nodes in the brain network. This raises the following questions. How does a non-zero $\bar{\Phi}$ emerge

370 spontaneously in the brain network? What is the network basis that facilitates the emergence of

371 a cause-effect structure? In this study, we propose that the phase lead-lag relationship that is

372 shaped by the structural brain network may create conditions that facilitate the emergence of a

373 cause-effect structure.

374 Previous studies have examined how brain network topology modulates the frequencies and

375 phases of local node dynamics, subsequently shaping a pattern of global information flow and

376 functional connectivity. A mathematical relationship between the node degree and the phase of
377 node dynamics was identified analytically [25,26], which enables us to estimate analytically the
378 phase of a node (in a functional network) with only its node degree and local connectivity (in a
379 structural network). This was tested with diverse brain networks (human, monkey, and mouse),
380 which demonstrated that when considering long-term and spatially coarse-grained brain
381 activities (> minutes) the global phase lead-lag relationship and information flow pattern
382 (measured by transfer entropy and Granger causality) were predictable based only on the
383 structural brain network topologies of the three species. In particular, the difference between the
384 "hub node" and "peripheral node" becomes most salient at a critical state. In other words, the
385 structural complexity of overall coupled node dynamics is maximized at a critical state. The
386 differences between frequency and phase among coupled node dynamics naturally give rise to
387 information flow in the brain network, consequently dividing the nodes in the brain network into
388 'senders' and 'receivers' of information flow. However, in sub- and supercritical states, there is
389 no information flow between node dynamics because of a highly-synchronized state (i.e., no
390 difference that would allow for information flow) and incoherent state (i.e., no interaction that
391 would allow for information flow). Therefore, a cause-effect structure may emerge between
392 these two extreme states and be maximized at a balanced state. Extrapolating from results
393 based on the phase lead-lag relationship, emerging a cause-effect structure without external
394 stimuli is likely not random but rather is organized by a mathematical relationship between
395 network structure and dynamics in a critical state [25,26,56,57].

396

397 **A large variation under a large constraint:** In our modeling study and EEG analysis, we found
398 that a large variation of the functional brain network occurs in spite of a strong constraint from
399 the structural brain network. Notably, the large variation and the strong constraint were
400 observed at different time scales. When we investigated the correlation coefficient between the
401 instantaneous phases and the node degrees of the 78 nodes, the correlation coefficient at each
402 time point varied widely at a short time scale (~ seconds) (Figure 3C). By contrast, the averaged
403 instantaneous phases and the node degrees at a longer time scale (~ minutes) have a large
404 positive correlation coefficient (r=0.57, Figure 3B), which implied a bias toward positive values in
405 the short time scale variation. Our previous EEG study demonstrated that the correlation
406 coefficient between the EEG network and the structural brain network was pronounced when
407 calculated with large temporal windows (> 60 seconds) but diminished when calculated with
408 small windows (< 5 seconds). Interestingly, the scale-dependency appeared only in the baseline

409   conscious states, not in the altered states of consciousness such as anesthetized state,

410   minimally conscious state, and unresponsive wakefulness syndrome [23]. The conscious brain

411   can be characterized by diverse repertoires of global functional connectivity on a short time

412   scale. However, when combining all repertoires of small windows in a large window, the

413   different functional connectivity patterns across small windows may be averaged out and only

414   the common functional connectivity patterns that are constrained by the structural brain network

415   remain. Such an averaged functional connectivity in a large window can be simulated by the

416   mean-field method upon a structural brain network. Nevertheless, how the large variance and

417   the large constraint contribute to the large integrated information in conscious states remains

418   elusive. Further studies are required to understand the mechanistic association between the

419   functional variance, structural constraint, and Φ in a network.

420

421   **Deviations from criticality and $\overline{\Phi}$:** When brain dynamics deviate from a critical state, the

422   capacity to shape global node dynamics into a structure that resembles the network structure is

423   lost. In a supercritical state, there is no functional interaction between nodes. In a subcritical

424   state, node dynamics cannot be structured due to strong functional interactions between nodes

425   that eliminate functional heterogeneity. As a result, the $\overline{\Phi}$ of a brain not in a critical

426   state—regardless of whether the deviation is toward subcriticality or supercriticality—will

427   decrease in proportion to the distance from the critical state.

428   Many empirical studies support the criticality hypothesis in consciousness by comparing the

429   dynamics of various conscious states with unconscious states (such as sleep, anesthesia,

430   seizure, and coma). They have commonly shown that unconsciousness is associated with a

431   deviation from criticality, which is quantified with various methods (power law, susceptibility, pair

432   correlation function, and correlation between the functional and structural brain networks)

433   [15,22,23,40,58–68]. However, no one has yet associated criticality, human consciousness, and

434   Φ because of the explosive computational demands required for Φ calculations. In a previous

435   study, we introduced a method that statistically estimates the increase/decrease of Φ for a

436   continuous EEG, termed $\overline{\Phi}$, and showed the applicability to characterizing levels of

437   consciousness with high-density EEG and also enabled us to study a relationship with network

438   criticality. Our current results show that the empirical and computational model studies support

439   the hypothesis that the characteristic network properties in a critical state naturally give rise to a

440   structured, asymmetric phase lead-lag relationship among oscillators and, in turn, maximize Φ

441   in the conscious brain.

442

443 **Limitations:** This study has several limitations**.** First, $\bar{\Phi}$ does not measure the precise Φ.
444 Instead, we estimated the relative change of Φ, focusing on the increase/decrease along with
445 the change in criticality in the network model and based on empirical EEG during anesthetic-
446 induced unconsciousness. Even so, this relative measure is sufficient for the purpose of this
447 study, which is to examine the relationship between Φ, criticality, and levels of consciousness.
448 And considering the significant differences among the six versions of Φ in the recent
449 comparison [69], testing our conclusion with other versions of Φ is required. Second, in this
450 study, we derived a relationship between asymmetric phase lead-lag relationships and $\bar{\bar{\Phi}}$, but
451 this relationship does not explain how the phase lead-lag relationship generates a cause-effect
452 relationship defined by information partition for Φ. It may require an analytic study to identify
453 conditions to link phase lead-lag and Φ. Third, to find an association between Φ, criticality, and
454 consciousness, we used the subjects' response rate during exposure to a general anesthetic as
455 a surrogate for the level of consciousness. However, it is well known that unresponsiveness
456 does not necessarily correlate with lack of consciousness. Although previously studied in the
457 context of vegetative and minimally conscious states, our research team has recently identified
458 covert consciousness during propofol sedation in which overt motoric responses were absent
459 but brain network responses suggestive of volition were present [70]. Future studies might
460 incorporate EEG data, behavioral responsiveness, and neuroimaging protocols to determine
461 covert consciousness in order to more precisely identify the relationship between critical
462 dynamics, consciousness, and Φ. Finally, the structural brain network used in the modeling
463 study includes only the cortex. Including subcortical networks such as thalamocortical and
464 hippocampocortical connections, etc. could improve the modeling performance for complex
465 state transitions during general anesthesia.

466

467 **Conclusion:** We demonstrated for the first time an explicit relationship between criticality,
468 integrated information, and human consciousness with computational modeling and EEG
469 analysis. We propose that network criticality, that is, a balanced state between large variation of
470 functional network configurations and strong constraint of structural network configurations, is a
471 network condition for integrated information. Understanding this relationship may open a new
472 way to study diverse states of consciousness situated near to and far from a critical state in
473 terms of integrated information. It may also provide a theoretical foundation for controlling the
474 level of consciousness and integrated information by modulating criticality at a network level.

475

478

References

480   1.   Oizumi M, Albantakis L, Tononi G. From the phenomenology to the mechanisms of

481   consciousness: Integrated Information Theory 3.0. PLoS Comput Biol. 2014;10:

482   e1003588. doi:10.1371/journal.pcbi.1003588

483   2.   Tononi G. An information integration theory of consciousness. BMC Neurosci. 2004;5: 42.

484   doi:10.1186/1471-2202-5-42

485   3.   Tononi G, Boly M, Massimini M, Koch C. Integrated information theory: from

486   consciousness to its physical substrate. Nat Rev Neurosci. 2016;17: 450–461.

487   doi:10.1038/nrn.2016.44

488   4.   Tononi G, Koch C. The neural correlates of consciousness: an update. Ann N Y Acad

489   Sci. 2008;1124: 239–261. doi:10.1196/annals.1440.004

490   5.   Tononi G. Integrated information theory of consciousness: an updated account. Arch Ital

491   Biol. 2012;150: 56–90. doi:10.4449/aib.v149i5.1388

492   6.   Tononi G. Information integration: its relevance to brain function and consciousness. Arch

493   Ital Biol. 2010;148: 299–322. doi:10.4449/AIB.V148I3.1224

494   7.   Bak P, Tang C, Wiesenfeld K. Self-organized criticality. Phys Rev A. 1988;38: 364–374.

495   doi:10.1103/PhysRevA.38.364

496   8.   Bak P, Paczuski M. Complexity, contingency, and criticality. Proc Natl Acad Sci U S A.

497   1995;92: 6689–96. doi:10.1073/pnas.92.15.6689

498   9.   Kitzbichler MG, Smith ML, Christensen SR, Bullmore E, Bak P, Paczuski M, et al.

499   Broadband criticality of human brain network synchronization. PLoS Comput Biol. 2009;5:

500   e1000314. doi:10.1371/journal.pcbi.1000314

501   10.   Werner G. Metastability, criticality and phase transitions in brain and its models.

502   Biosystems. 2007;90: 496–508. doi:10.1016/J.BIOSYSTEMS.2006.12.001

503   11.   Hesse J, Gross T. Self-organized criticality as a fundamental property of neural systems.
504   Front Syst Neurosci. 2014;8: 166. doi:10.3389/fnsys.2014.00166

505   12.   Tagliazucchi E, Balenzuela P, Fraiman D, Chialvo DR. Criticality in large-scale brain
506   FMRI dynamics unveiled by a novel point process analysis. Front Physiol. 2012;3: 15.
507   doi:10.3389/fphys.2012.00015

508   13.   Hidalgo J, Grilli J, Suweis S, Muñoz MA, Banavar JR, Maritan A. Information-based
509   fitness and the emergence of criticality in living systems. Proc Natl Acad Sci. 2014;111:
510   10095–10100. doi:10.1073/PNAS.1319166111

511   14.   Haimovici A, Tagliazucchi E, Balenzuela P, Chialvo DR. Brain organization into resting
512   state networks emerges at criticality on a model of the human connectome. Phys Rev
513   Lett. 2013;110: 178101. doi:10.1103/PhysRevLett.110.178101

514   15.   Marinazzo D, Pellicoro M, Wu G, Angelini L, Cortés JM, Stramaglia S. Information
515   transfer and criticality in the Ising model on the human connectome. PLoS One. 2014;9:
516   e93616. doi:10.1371/journal.pone.0093616

517   16.   Moon J-Y, Lee U, Blain-Moraes S, Mashour GA. General relationship of global topology,
518   local dynamics, and directionality in large-scale brain networks. PLoS Comput Biol.
519   2015;11: e1004225. doi:10.1371/journal.pcbi.1004225

520   17.   Cocchi L, Gollo LL, Zalesky A, Breakspear M. Criticality in the brain: a synthesis of
521   neurobiology, models and cognition. Prog Neurobiol. 2017;158: 132–152.
522   doi:10.1016/J.PNEUROBIO.2017.07.002

523   18.   Beggs JM. The criticality hypothesis: how local cortical networks might optimize
524   information processing. Philos Trans R Soc A Math Phys Eng Sci. 2008;366: 329–343.
525   doi:10.1098/rsta.2007.2092

526   19.   Khajehabdollahi S, Abeyasinghe PM, Owen AM, Soddu A. The emergence of integrated
527   information, complexity, and consciousness at criticality. bioRxiv. 2019; 521567.
528   doi:10.1101/521567

529   20.   Kim M, Mashour GA, Moraes S-B, Vanini G, Tarnal V, Janke E, et al. Functional and
530   topological conditions for explosive synchronization develop in human brain networks
531   with the onset of anesthetic-induced unconsciousness. Front Comput Neurosci. 2016;10:
532   1. doi:10.3389/fncom.2016.00001

533   21.   Kim M, Kim S, Mashour GA, Lee U. Relationship of topology, multiscale phase
534   synchronization, and state transitions in human brain networks. Front Comput Neurosci.
535   2017;11: 55. doi:10.3389/fncom.2017.00055

536   22.   Beggs JM, Timme N. Being critical of criticality in the brain. Front Physiol. 2012;3: 163.
537   doi:10.3389/fphys.2012.00163

538   23.   Lee H, Golkowski D, Jordan D, Berger S, Ilg R, Lee J, et al. Relationship of critical
539   dynamics, functional connectivity, and states of consciousness in large-scale human
540   brain networks. Neuroimage. 2019;188: 228–238.
541   doi:10.1016/J.NEUROIMAGE.2018.12.011

542   24.   Yoon S, Sorbaro Sindaci M, Goltsev A V, Mendes JFF. Critical behavior of the relaxation
543   rate, the susceptibility, and a pair correlation function in the Kuramoto model on scale-
544   free networks. Phys Rev E. 2015;91: 32814. doi:10.1103/PhysRevE.91.032814

545   25.   Moon J-Y, Lee U, Blain-Moraes S, Mashour GA. General relationship of global topology,
546   local dynamics, and directionality in large-scale brain networks. PLoS Comput Biol.
547   2015;11: e1004225. doi:10.1371/journal.pcbi.1004225

548   26.   Moon J-Y, Kim J, Ko T-W, Kim M, Iturria-Medina Y, Choi J-H, et al. Structure shapes
549   dynamics and directionality in diverse brain networks: mathematical principles and
550   empirical confirmation in three species. Sci Rep. 2017;7: 46606. doi:10.1038/srep46606

551   27.   Breakspear M. Dynamic models of large-scale brain activity. Nat Neurosci. 2017;20: 340–
552   352. doi:10.1038/nn.4497

553   28.   Gong G, He Y, Concha L, Lebel C, Gross DW, Evans AC, et al. Mapping anatomical
554   connectivity patterns of human cerebral cortex using in vivo diffusion tensor imaging
555   tractography. Cereb Cortex. 2009;19: 524–536. doi:10.1093/cercor/bhn102

556   29.   Naruse Y, Matani A, Miyawaki Y, Okada M. Influence of coherence between multiple
557   cortical columns on alpha rhythm: a computational modeling study. Hum Brain Mapp.
558   2009;31: 703–715. doi:10.1002/hbm.20899

559   30.   Breakspear M, Heitmann S, Daffertshofer A. Generative models of cortical oscillations:
560   neurobiological implications of the kuramoto model. Front Hum Neurosci. 2010;4: 190.
561   doi:10.3389/fnhum.2010.00190

562   31.   Nakagawa TT, Woolrich M, Luckhoo H, Joensson M, Mohseni H, Kringelbach ML, et al.

563   How delays matter in an oscillatory whole-brain spiking-neuron network model for MEG

564   alpha-rhythms at rest. Neuroimage. 2014;87: 383–394.

565   doi:10.1016/J.NEUROIMAGE.2013.11.009

566 32. Flores FJ, Hartnack KE, Fath AB, Kim S-E, Wilson MA, Brown EN, et al. Thalamocortical

567   synchronization during induction and emergence from propofol-induced

568   unconsciousness. Proc Natl Acad Sci U S A. 2017;114: E6660–E6668.

569   doi:10.1073/pnas.1700148114

570 33. Deco G, Cabral J, Saenger VM, Boly M, Tagliazucchi E, Laufs H, et al. Perturbation of

571   whole-brain dynamics in silico reveals mechanistic differences between brain states.

572   Neuroimage. 2018;169: 46–56. doi:10.1016/j.neuroimage.2017.12.009

573 34. Deco G, Cabral J, Woolrich MW, Stevner ABA, van Hartevelt TJ, Kringelbach ML. Single

574   or multiple frequency generators in on-going brain activity: A mechanistic whole-brain

575   model of empirical MEG data. Neuroimage. 2017;152: 538–550.

576   doi:10.1016/J.NEUROIMAGE.2017.03.023

577 35. Jobst BM, Hindriks R, Laufs H, Tagliazucchi E, Hahn G, Ponce-Alvarez A, et al.

578   Increased stability and breakdown of brain effective connectivity during slow-wave sleep:

579   mechanistic insights from whole-brain computational modelling. Sci Rep. 2017;7: 4634.

580   doi:10.1038/s41598-017-04522-x

581 36. Kim M, Kim S, Mashour GA, Lee U. Relationship of topology, multiscale phase

582   synchronization, and state transitions in human brain networks. Front Comput Neurosci.

583   2017;11: 55. doi:10.3389/fncom.2017.00055

584 37. Zhang H, Watrous AJ, Patel A, Jacobs J. Theta and alpha oscillations are traveling

585   waves in the human neocortex. Neuron. 2018;98: 1269–1281.e4.

586   doi:10.1016/j.neuron.2018.05.019

587 38. Caminiti R, Ghaziri H, Galuske R, Hof PR, Innocenti GM. Evolution amplified processing

588   with temporally dispersed slow neuronal connectivity in primates. Proc Natl Acad Sci U S

589   A. 2009;106: 19551–19556. doi:10.1073/pnas.0907655106

590 39. Blain-Moraes S, Tarnal V, Vanini G, Alexander A, Rosen D, Shortal B, et al.

591   Neurophysiological correlates of sevoflurane-induced unconsciousness. Anesthesiology.

592   2015;122: 307–316. doi:10.1097/ALN.0000000000000482

593   40.   Beggs JM, Plenz D. Neuronal avalanches in neocortical circuits. J Neurosci. 2003;23:
594   11167–77. doi:10.1523/JNEUROSCI.23-35-11167.2003

595   41.   Brochini L, de Andrade Costa A, Abadi M, Roque AC, Stolfi J, Kinouchi O. Phase
596   transitions and self-organized criticality in networks of stochastic spiking neurons. Sci
597   Rep. 2016;6: 35831. doi:10.1038/srep35831

598   42.   Kim H, Moon J-Y, Mashour GA, Lee U. Mechanisms of hysteresis in human brain
599   networks during transitions of consciousness and unconsciousness: Theoretical
600   principles and empirical evidence. PLOS Comput Biol. 2018;14: e1006424.
601   doi:10.1371/journal.pcbi.1006424

602   43.   Lv P, Guo L, Hu X, Li X, Jin C, Han J, et al. Modeling dynamic functional information
603   flows on large-scale brain networks. Med Image Comput Comput Assist Interv. 2013;16:
604   698–705.

605   44.   Schmidt R, LaFleur KJR, de Reus MA, van den Berg LH, van den Heuvel MP. Kuramoto
606   model simulation of neural hubs and dynamic synchrony in the human cerebral
607   connectome. BMC Neurosci. 2015;16. doi:10.1186/s12868-015-0193-z

608   45.   Deco G, Kringelbach ML, Jirsa VK, Ritter P. The dynamics of resting fluctuations in the
609   brain: metastability and its dynamical cortical core. Sci Rep. 2017;7: 3095.
610   doi:10.1038/s41598-017-03073-5

611   46.   Stanley HE, Wong VK. Introduction to phase transitions and critical phenomena. Am J
612   Phys. 1972;40: 927–928. doi:10.1119/1.1986710

613   47.   Oizumi M, Tsuchiya N, Amari S. Unified framework for information integration based on
614   information geometry. Proc Natl Acad Sci U S A. 2016;113: 14817–14822.
615   doi:10.1073/pnas.1603583113

616   48.   Barrett AB, Seth AK. Practical Measures of Integrated Information for Time-Series Data.
617   PLoS Comput Biol. Public Library of Science; 2011;7: e1001052.
618   doi:10.1371/journal.pcbi.1001052

619   49.   Kim H, Hudetz AG, Lee J, Mashour GA, Lee U, Group the RS, et al. Estimating the
620   integrated information measure Phi from high-density electroencephalography during
621   states of consciousness in humans. Front Hum Neurosci. 2018;12: 42.
622   doi:10.3389/FNHUM.2018.00042

623   50.   Stam CJ, Nolte G, Daffertshofer A. Phase lag index: assessment of functional
624   connectivity from multi channel EEG and MEG with diminished bias from common
625   sources. Hum Brain Mapp. 2007;28: 1178–1193. doi:10.1002/hbm.20346

626   51.   Lee U, Lee H, Müller M, Noh G-J, Mashour GA. Genuine and spurious phase
627   synchronization strengths during consciousness and general anesthesia. PLoS One.
628   2012;7: e46313. doi:10.1371/journal.pone.0046313

629   52.   Wen P, Li Y. EEG human head modelling based on heterogeneous tissue conductivity.
630   Australas Phys Eng Sci Med. 2006;29: 235–240. doi:10.1007/BF03178571

631   53.   Oostenveld R, Fries P, Maris E, Schoffelen J-M. FieldTrip: open source software for
632   advanced analysis of MEG, EEG, and invasive electrophysiological data. Comput Intell
633   Neurosci. 2011;2011: 156869. doi:10.1155/2011/156869

634   54.   Deco G, Jirsa VK. Ongoing cortical activity at rest: criticality, multistability, and ghost
635   attractors. J Neurosci. 2012;32: 3366–75. doi:10.1523/JNEUROSCI.2523-11.2012

636   55.   Tagliazucchi E, Chialvo DR, Siniatchkin M, Amico E, Brichant J-F, Bonhomme V, et al.
637   Large-scale signatures of unconsciousness are consistent with a departure from critical
638   dynamics. J R Soc Interface. 2016;13: 20151027. doi:10.1098/rsif.2015.1027

639   56.   Hu X, Boccaletti S, Huang W, Zhang X, Liu Z, Guan S, et al. Exact solution for first-order
640   synchronization transition in a generalized Kuramoto model. Sci Rep. 2014;4: 7262.
641   doi:10.1038/srep07262

642   57.   Ko T-W, Ermentrout GB. Partially locked states in coupled oscillators due to
643   inhomogeneous coupling. Phys Rev E Stat Nonlin Soft Matter Phys. 2008;78: 16203.
644   doi:10.1103/PhysRevE.78.016203

645   58.   Bédard C, Destexhe A. Macroscopic models of local field potentials and the apparent 1/f
646   noise in brain activity. Biophys J. 2009;96: 2589–2603. doi:10.1016/J.BPJ.2008.12.3951

647   59.   Hudetz AG, Humphries CJ, Binder JR. Spin-glass model predicts metastable brain states
648   that diminish in anesthesia. Front Syst Neurosci. 2014;8: 234.
649   doi:10.3389/fnsys.2014.00234

650   60.   Liang Z, King J, Zhang N. Intrinsic organization of the anesthetized brain. J Neurosci.
651   2012;32: 10183–10191. doi:10.1523/JNEUROSCI.1020-12.2012

652 61. Liu X, Ward BD, Binder JR, Li S-J, Hudetz AG. Scale-free functional connectivity of the
653   brain is maintained in anesthetized healthy participants but not in patients with
654   unresponsive wakefulness syndrome. PLoS One. 2014;9: e92182.
655   doi:10.1371/journal.pone.0092182

656 62. Lee U, Mashour GA. Role of network science in the study of anesthetic state transitions.
657   Anesthesiology. 2018; 1. doi:10.1097/ALN.0000000000002228

658 63. Moretti P, Muñoz MA. Griffiths phases and the stretching of criticality in brain networks.
659   Nat Commun. 2013;4: 2521. doi:10.1038/ncomms3521

660 64. Priesemann V, Valderrama M, Wibral M, Le Van Quyen M. Neuronal avalanches differ
661   from wakefulness to deep sleep – evidence from intracranial depth recordings in humans.
662   PLoS Comput Biol. 2013;9: e1002985. doi:10.1371/journal.pcbi.1002985

663 65. Lee U, Oh G, Kim S, Noh G, Choi B, Mashour GA. Brain networks maintain a scale-free
664   organization across consciousness, anesthesia, and recovery: evidence for adaptive
665   reconfiguration. Anesthesiology. 2010;113: 1081–1091.
666   doi:10.1097/ALN.0b013e3181f229b5

667 66. Krzemiński D, Kamiński M, Marchewka A, Bola M. Breakdown of long-range temporal
668   correlations in brain oscillations during general anesthesia. Neuroimage. 2017;159: 146–
669   158. doi:10.1016/J.NEUROIMAGE.2017.07.047

670 67. Meisel C, Storch A, Hallmeyer-Elgner S, Bullmore E, Gross T. Failure of adaptive self-
671   organized criticality during epileptic seizure attacks. PLoS Comput Biol. 2012;8:
672   e1002312. doi:10.1371/journal.pcbi.1002312

673 68. Bonachela JA, de Franciscis S, Torres JJ, Muñoz MA. Self-organization without
674   conservation: are neuronal avalanches generically critical? J Stat Mech Theory Exp.
675   2010;2010: P02015. doi:10.1088/1742-5468/2010/02/P02015

676 69. Mediano P, Seth A, Barrett A, Mediano PAM, Seth AK, Barrett AB. Measuring integrated
677   information: comparison of candidate measures in theory and simulation. Entropy.
678   2018;21: 17. doi:10.3390/e21010017

679 70. Huang Z, Vlisides PE, Tarnal VC, Janke EL, Keefe KM, Collins MM, et al. Brain imaging
680   reveals covert consciousness during behavioral unresponsiveness induced by propofol.
681   Sci Rep. 2018;8: 13195. doi:10.1038/s41598-018-31436-z